TU Delft

Delft University of Technology

Rapid quality control for recycled coarse aggregates (RCA) streams

Multi-sensor integration for advanced contaminant detection

Chang, Cheng; Di Maio, Francesco; Bheemireddy, Rajeev; Posthoorn, Perry; Gebremariam, Abraham T.; Rem, Peter

DOI
10.1016/j.compind.2024.104196

Publication date
2024

Document Version
Final published version

Published in
Computers in Industry

Citation (APA)
Chang, C., Di Maio, F., Bheemireddy, R., Posthoorn, P., Gebremariam, A. T., & Rem, P. (2024). Rapid quality control for recycled coarse aggregates (RCA) streams: Multi-sensor integration for advanced contaminant detection. *Computers in Industry*, *164*, Article 104196. https://doi.org/10.1016/j.compind.2024.104196

Important note
To cite this publication, please use the final published version (if applicable).
Please check the document version above.

Copyright
Other than for strictly personal use, it is not permitted to download, forward or distribute the text or part of it, without the consent of the author(s) and/or copyright holder(s), unless the work is under an open content license such as Creative Commons.

Takedown policy
Please contact us and provide details if you believe this document breaches copyrights.
We will remove access to the work immediately and investigate your claim.

This work is downloaded from Delft University of Technology.
For technical reasons the number of authors shown on this cover page is limited to a maximum of 10.

Computers in Industry 164 (2025) 104196

Contents lists available at ScienceDirect

Computers in Industry

journal homepage: www.sciencedirect.com/journal/computers-in-industry

Rapid quality control for recycled coarse aggregates (RCA) streams: Multi-sensor integration for advanced contaminant detection

Cheng Chang [a,*], Francesco Di Maio [a], Rajeev Bheemireddy [b], Perry Posthoorn [b], Abraham T. Gebremariam [a], Peter Rem [a]

[a] Resource & Recycling, Department of Engineering Structures, Faculty of Civil Engineering and Geosciences, Delft University of Technology, Stevinweg 1, Delft 2628 CN, the Netherlands

[b] DEMO, Delft University of Technology, Gebouw 36, Mekelweg 4, Delft 2628 CD, the Netherlands

ARTICLE INFO

Keywords:
Laser-Induced Breakdown Spectroscopy (LIBS)
Recycled Coarse Aggregates (RCA)
Object Detection
Surface Condition Adaptation
3D scanning
Quality Control

ABSTRACT

Recycling coarse aggregates from construction and demolition waste is essential for sustainable construction practices. However, the quality of recycled coarse aggregates (RCA) often fluctuates significantly, in contrast to the more stable quality of natural aggregates. Contaminants in RCA notably compromise its quality and usability. Therefore, automating the quality control of RCA is necessary for the recycling industry. This study introduces an industry-focused, innovative, and rapid quality control system that combines Laser-Induced Breakdown Spectroscopy (LIBS) with 3D scanning technologies to enhance the detection of contaminants in RCA streams. The system involves a synchronized application of LIBS for spectral analysis and 3D scanning for the physical characterization of different materials. Results reveal that the dependability of single-shot LIBS analysis has been enhanced, thus elevating the precision of contaminant detection. This improvement is achieved by accounting for the laser shot's angle of incidence and focal length adjustments. The introduced technology holds potential for application in the real-time examination of substantial volumes of RCA, facilitating a rapid and reliable quality control method. This rapid assessment technique delivers online data about the concentration of contaminants in RCA, including recycled fine aggregates, cement paste, bricks, foam, glass, gypsum, mineral fibers, plastics, and wood. This data is both essential and sufficient for choosing a cost-effective mortar recipe and guaranteeing the performance of the final concrete product in terms of strength and durability in construction projects. The system can monitor the quality of RCA flows at throughputs of 50 tons per hour per conveyor, characterizing approximately 4000 particles in every ton of RCA, in this way signaling the most critical contaminants at levels of less than 50 parts per million. With these characteristics, the system could also become relevant for other applications, such as characterizing mining waste or solid biofuels for power plants.

1. Introduction

The global shift towards sustainable construction practices has increasingly emphasized the importance of recycling materials, particularly in the context of construction and demolition waste. Among these materials, recycled coarse aggregates (RCA) are of significant interest due to their potential to reduce environmental impact and contribute to resource conservation (de Andrade Salgado and de Andrade Silva, 2022; Silva et al., 2017). The quality of the aggregate improves with more thorough waste treatment (Martín-Morales et al., 2011). Despite its potential, the effective recycling of RCA is hampered by significant challenges in accurately detecting contaminants, a crucial step to ensure the quality and safety of recycled materials.

The challenge primarily arises from the frequent and significant fluctuations in RCA quality (Lux et al., 2023). While RCA offer significant environmental benefits by reducing the demand for natural resources and minimizing construction waste, they exhibit distinct properties that differentiate them from natural aggregates. These differences, which include variations in porosity, absorption, and surface texture, can influence the mechanical properties and durability of concrete made with RCA (He et al., 2024). Natural aggregates originate from relatively uniform geological sources, maintaining stable quality over long periods. In contrast, RCA quality can exhibit considerable fluctuations over relatively short intervals due to the diverse nature of

* Corresponding author.
E-mail addresses: C.Chang-1@tudelft.nl, chang-cheng@outlook.com (C. Chang).

https://doi.org/10.1016/j.compind.2024.104196
Received 5 August 2024; Received in revised form 9 September 2024; Accepted 30 September 2024
0166-3615/© 2024 The Author(s). Published by Elsevier B.V. This is an open access article under the CC BY-NC-ND license (http://creativecommons.org/licenses/by-nc-nd/4.0/).

demolition waste. Such waste includes materials from different sections of various demolition sites and is processed with differences in recycling methods. Therefore, the non-uniform composition and properties of the input demolition waste directly influences the uniformity of the resulting RCA.

Research on RCA has predominantly examined how contaminants affect concrete quality (Abid et al., 2018; Ahmad et al., 2023; Bai et al., 2020). However, precise detection and classification of these contaminants in RCA have received less attention. Vegas et al. analyzed mixed recycled aggregates from various European countries, revealing that near-infrared sorting effectively reduces, if not eliminates, problematic fractions (Vegas et al., 2015). Serranti and Bonifazi developed strategies to detect asbestos-containing materials and other contaminants in concrete aggregates derived from demolition waste (Serranti and Bonifazi, 2020). Xia and Bakker examined different material particle samples, concluding that the success of practical testing depends on the training set's quality and the management of potential false positives (Xia and Bakker, 2014). Despite these advancements, a significant gap remains in methods for in-situ evaluation of contaminants in RCA, particularly their application in industrial scenarios (Bonifazi et al., 2018; Serranti et al., 2023).

A primary challenge in the field of recycling RCA remains the accurate detection of contaminants that might evade initial sorting processes. This is particularly crucial in quality control, where even a small percentage of undetected contaminants can compromise the final product's integrity. False positives in sorting are less critical, as they result in acceptable losses of non-contaminated material. However, the accurate detection and minimization of false positives in quality control are essential to ensure the reliability and high quality of the recycled aggregates. A high rate of false positives can lead to RCA being mistakenly identified as contaminated, which can diminish the quality and value of what was originally high-quality and valuable material. Currently, the field lacks a rapid and precise method for detecting a wide range of contaminants in RCA. This gap is largely due to the inconsistent and unpredictable nature of these contaminants. These inconsistencies hinder the accurate detection of contaminants, complicating the development of a universal, straightforward method for detecting all contaminants. Consequently, this leads to considerable discrepancies in the quality assessments of RCA. In various engineering fields, quality control systems have been extensively employed to ensure precision and reliability (Caiazzo et al., 2022; Güvenç et al., 2023; Suthar et al., 2023). However, the challenges associated with RCA differ significantly from those in conventional engineering processes. Addressing these challenges requires the adoption of efficient, reliable, non-destructive, and cost-effective sensor technologies. Such technologies would enable automatic contaminant detection, addressing the diverse nature of recycled materials. Implementing this approach will enhance quality control in the use of RCA, ensuring a more consistent and reliable end product.

Laser-induced breakdown spectroscopy (LIBS) is emerging as a highly promising technology for real-time, on-site elemental analysis, particularly within the expansive market of concrete production industries (Mansoori et al., 2011; Yin et al., 2016). LIBS offers numerous advantages for practical operations, including minimal or no sample preparation, real-time analysis, and comprehensive element measurement capabilities (Wang et al., 2021). In the concrete sector, LIBS is commonly employed for both identifying and quantifying chemical elements (qualitative and quantitative) (Cabral et al., 2023). However, its application in classifying, recognizing, and recycling various construction materials remains underexplored (Chang et al., 2022; Elfaham and Eldemerdash, 2019; Xia and Bakker, 2014). Gottlieb et al. introduced an algorithm for heterogeneous concrete to isolate spectral data of non-relevant aggregates and cement matrix (Gottlieb et al., 2017). Völker et al. investigated cement paste prisms to distinguish cement types and noted that additional moisture changes the laser material interaction and the composition of vaporized material volume, affecting classification (Völker et al., 2020). Živković et al. used LIBS with microscopic-scale spatial resolution to map elemental distribution in archaeological samples from the Smederevo Fortress, Serbia (Živković et al., 2021). JIA et al. noted that in the cement industry, the matrix of the cement raw meal varies due to different sources, possibly extending beyond the calibration sample concentration range (Jia et al., 2019). Most studies are confined to laboratory environments, emphasizing the need for environmental considerations during measurements (Dietz et al., 2019; Mansoori et al., 2011). Hence, practical application in concrete industrial production is limited.

A significant challenge for LIBS in quantitative measurements is its relatively high uncertainty or low repeatability (Wang et al., 2021). This uncertainty in collected spectral data significantly impacts classification accuracy. This is due to various factors, but most research work was concentrated superficially on the impact of different system parameters on the emission signals (Kim et al., 2013; Wang et al., 2020), temperatures (Palanco et al., 1999) and ambient gas (Yu et al., 2020) on LIBS performance. While many algorithms have been developed to classify materials using LIBS, less attention has been given to surface information analysis to enhance spectral signals. Zhang et al. found that adjusting lens-to-sample distances improves LIBS's analytical performance, enhancing precision and detection limits (Zhang et al., 2012). Wang et al. investigated the effect of surface roughness on solid samples, concluding that preparing smooth surfaces leads to more consistent laser-sample interactions and fewer plasma fluctuations (Wang et al., 2021). However, in practical scenarios, the uneven surfaces of materials like RCA pose challenges for LIBS to obtain high-quality spectral information.

This study presents an innovative and rapid quality control system that enhances contaminant detection precision in RCA streams by employing surface-condition-adaptive LIBS. This advancement results from merging LIBS with 3D scanning technology, providing vital data on surface conditions at each laser shooting point. Consequently, this integration substantially enhances the reliability of analytical results obtained from each single LIBS laser shot. For effective operation, precise synchronization and calibration of the two sensors are essential. The technique involves a detailed analysis of the LIBS laser focal length and angle of incidence at the shooting point. The process continues by filtering the collected spectral data, omitting laser shots that do not meet the required standards. Then, both the angles of incidence and corresponding spectral values are incorporated into the cluster-based classification algorithm. This approach allows the LIBS system to dynamically adjust its analysis according to the real-time surface conditions encountered during each laser shot. This adjustment process enhances the quality of the laser shot and reduces the false-positive rates in material misclassification. By adopting this adaptive strategy, the accuracy of detecting various contaminants in RCA is improved. Key performance metrics, such as precision, recall, and F1-score (all weighted averages), reach 0.99. This high level of accuracy in turn supports rapid and reliable quality control of RCA streams on the conveyor belt. The research thoroughly assesses this surface-condition-adaptive LIBS method, highlighting its proficiency in precisely identifying a variety of materials commonly encountered in construction waste. Fig. 1 illustrates the procedural flowchart, offering a visual summary of the methodological sequence employed in this study.

2. Materials and methods

2.1. Materials

Demolition waste samples (Fig. 2) were gathered from sites in the Netherlands for analysis. Distinct materials (bricks, foam, glass, gypsum, mineral fibers, plastics, and wood) were separated either by hand or with the help of inline sorters available at the recycling facility. The End-of-Life (EoL) concrete was obtained relatively clean through selective demolition. This EoL concrete was then processed using the Concrete to

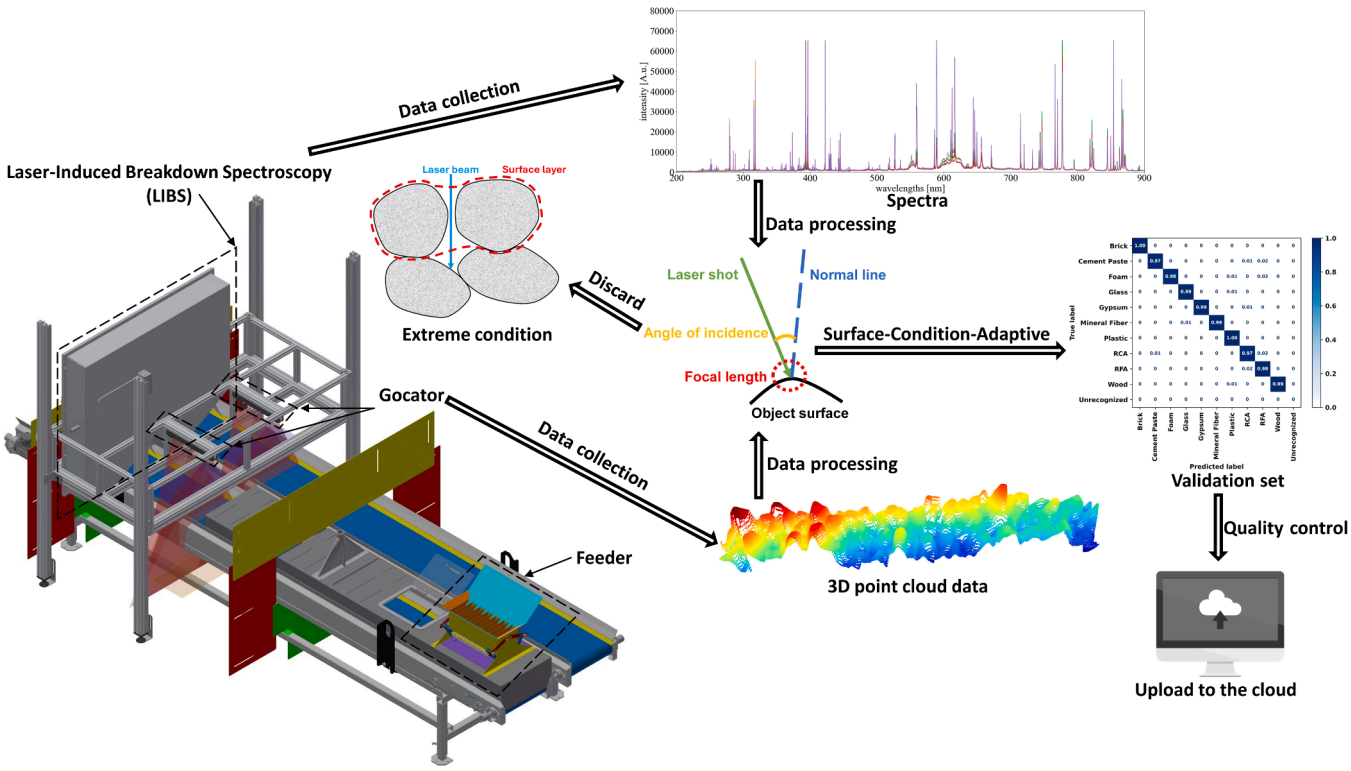

Fig. 1. Schematic of quality control process.

Fig. 2. Demolition waste samples.

Cement and Aggregate (C2CA) technology (Gebremariam et al., 2020). The output was divided into three categories: RCA ranging from 4.0 to 16.0 mm, recycled fine aggregates (RFA) between 0.25 and 4.0 mm, and cement paste-rich powder sized 0 to 0.25 mm. This is accomplished using the Advanced Dry Recovery (ADR) and Heating Air classification System (HAS) technologies (Gebremariam et al., 2020). These technologies are specifically to segregate EoL concrete into well-defined particle size distributions based on mechanical and thermal processing methods.

2.2. Equipment

2.2.1. Sensor-based quality control system

The sensor-based quality control system depicted in Fig. 3 begins with the process of transporting the to-be-inspected objects via a feeder to the conveyor belt, which then conveys them under the sensor system for analysis. This system encompasses two principal sensors: the 3D scanner Gocator and the LIBS. Both sensors are mounted on a fixed frame directly above the conveyor belt. The LIBS is aligned perpendicularly to the direction of the conveyor belt's movement, while the

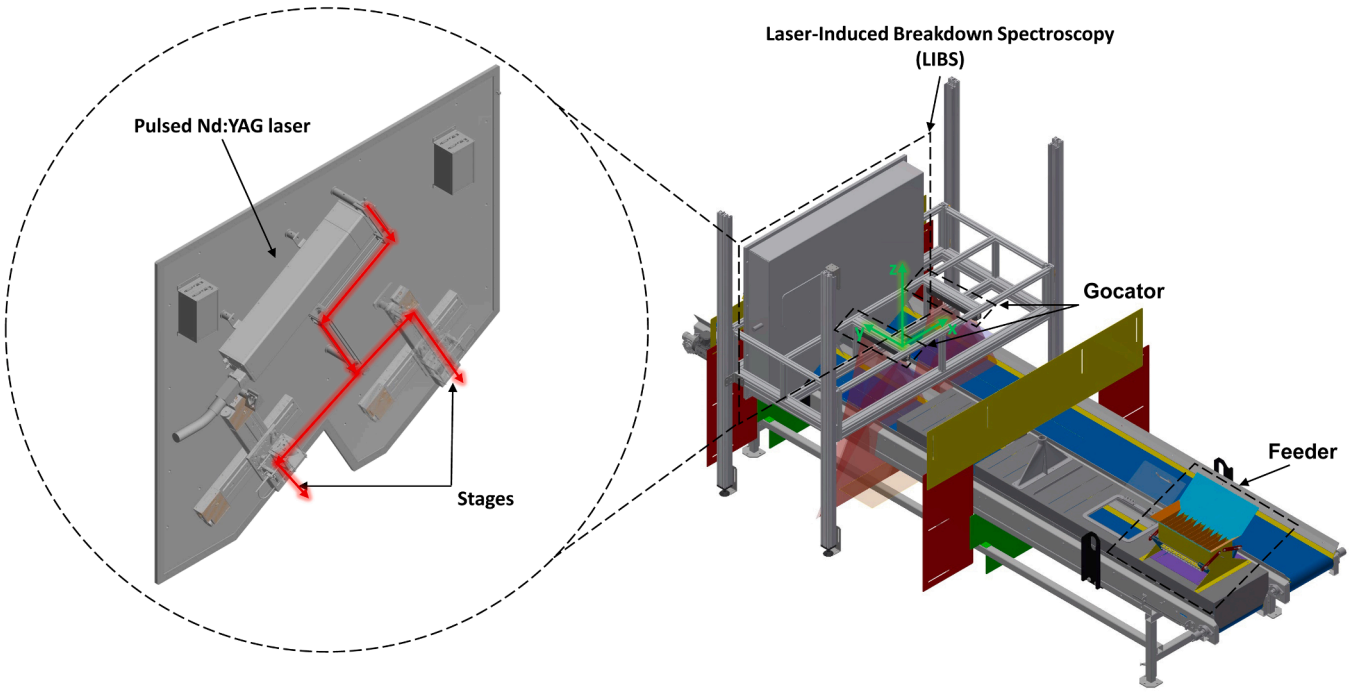

Fig. 3. Sensor-based quality control system.

Gocator is oriented parallel to it. The Gocator specializes in detecting the surface conditions of target objects, generating high-resolution (x-direction: 0.378 mm, y-direction: 0.393 mm, z-direction: 0.083 mm), three-dimensional point cloud data that effectively captures the detailed surface topography. On the other hand, LIBS plays a pivotal role in the recognition and classification of various objects.

A distinctive feature of the system's design is the integration of multiple reflective mirrors. The laser beam is divided and directed using a series of beam splitters and mirrors (as shown by the red arrows in Fig. 3) onto two separate conveyor belts. To further fine-tune the position of the laser beam, a dual-stage system is employed, with each stage directing a laser beam to one of the conveyor belts. The laser's position can be adjusted based on the specific characteristics of the objects being inspected. The laser beams' positioning can be adjusted according to the specific attributes of the objects being inspected. This design enables the simultaneous monitoring of objects on two distinct conveyor belts using just a single Nd: TAG laser.

2.2.2. Synchronization

To enhance spectral analysis through surface information, it is crucial to synchronize the two sensors. This approach enables enhancement of the analysis of spectra obtained from LIBS by incorporating surface conditions of the target points captured by the Gocator. An integrated encoder is employed for the control and logging of the conveyor belt, Gocator, and LIBS systems. The integrated encoder's resolution is set at 4098 pulses per revolution. Given the conveyor belt's wheel perimeter of 402.116 mm, the belt advances 0.098 mm with each pulse of the integrated encoder. Considering the maximum scanning frequency of the Gocator, its internal encoder resolution is configured at 1024 pulses per revolution. This implies that for every four pulses emitted by the integrated encoder, the Gocator executes one scan. Consequently, the calculated resolution of the Gocator along the conveyor belt's direction of travel is 0.393 mm.

Experimental data indicates a horizontal distance of 6025 integrated encoder pulses, equivalent to 591.203 mm, between the linear scans of the Gocator and the LIBS laser shooting point. Based on this, synchronization of the Gocator and LIBS signals is achieved through the pulse values recorded by the integrated encoder. When the LIBS emits a laser shot, the corresponding pulse value of LIBS recorded by the integrated encoder at that moment is *pv*. Therefore, the surface targeted at that instant corresponds to the (*pv*-6025)/4 scan in the Gocator's dataset.

2.2.3. Calibration

Within this setup, two sensors have been securely mounted on the same frame. The LIBS is oriented vertically, while the Gocator sensor maintains a horizontal position and is perpendicular to the plane of the LIBS (as shown in Fig. 4). The relative positioning of the sensors has been precisely pre-calibrated, ensuring no displacement occurs between them. The conveyor belt, however, is distinct and separate from this frame. In practice, the conveyor belt is inserted beneath the frame to align with the operation of the sensors. Should the positioning be incorrect, recalibration is required to ensure accuracy.

To enhance clarity, a spatial coordinate system, as illustrated in Fig. 3, is established. The x-axis is defined as the direction perpendicular to the Gocator body, pointing towards the direction of the conveyor belt's movement. The y-axis runs parallel to the Gocator body, and the z-axis is oriented vertically upwards from the Gocator body.

To address misalignments between the sensor system and the conveyor belt, which can introduce measurement inaccuracies, a calibration methodology is necessary. Specifically, in practical operations, the conveyor belt does not maintain a perfect horizontal position and deviates from the ideal alignment along the z-axis, as well as exhibits variations along the x and y-axes. The correction approach involves the use of a flat calibration plate placed on the conveyor belt. Two arbitrary points labeled A and B, are selected on the plate, ensuring that their y-axis coordinates are not identical. The differences along the x-axis (Δx) and the y-axis (Δy) between points A and B are recorded.

As the conveyor belt operates, the calibration plate undergoes scanning by the Gocator. Initially, the Gocator captures the coordinates of point A (x_a, y_a, z_a). After a span of number t pulses, the Gocator records the coordinates of point B (x_b, y_b, z_b). The respective differences in the coordinates of points A and B are then calculated as follows:

$$\begin{cases} \Delta x' = x_b - x_a \\ \Delta y' = y_b - y_a \\ \Delta z' = z_b - z_a \end{cases} \quad (1)$$

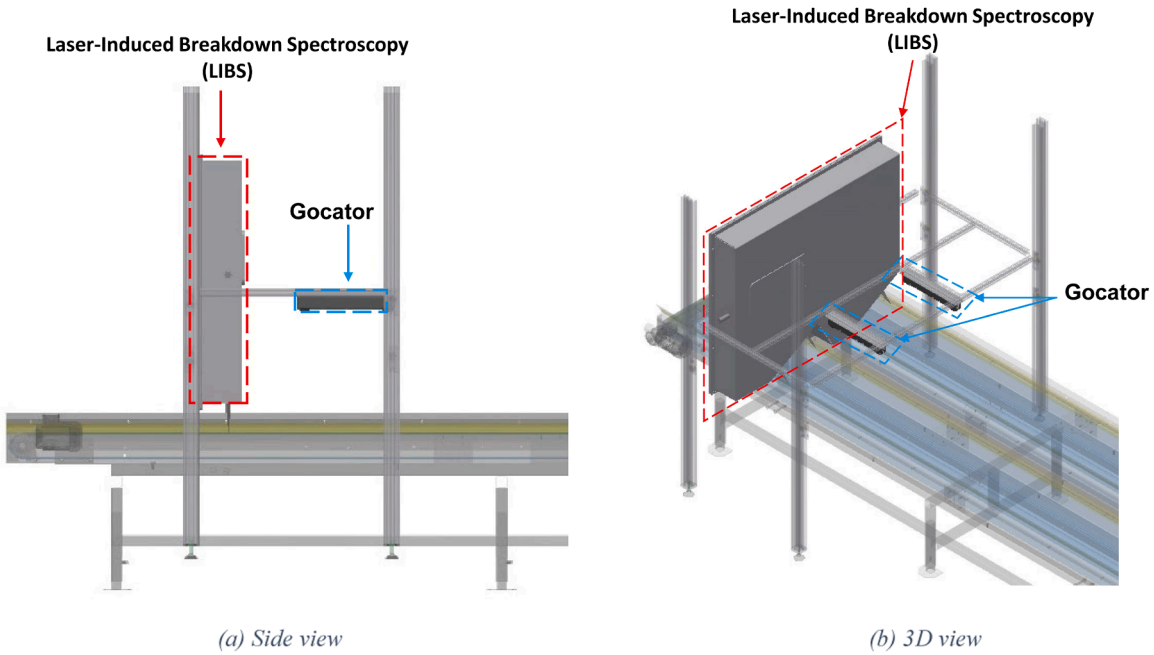

Fig. 4. Pre-calibrated sensors.

If the conveyor belt is positioned correctly, it should satisfy the following relationships:

$$\begin{cases} \Delta x' = \Delta x \\ \Delta y' = \Delta y \\ \Delta z' = 0 \end{cases} \tag{2}$$

If the relationships are not satisfied, this indicates a misalignment in the placement of the conveyor belt, necessitating an adjustment. Referring to Equation Set (3), the values for the offset in each pulse along the x, y, and z axes (ε_x, ε_y, ε_z) can be accurately calculated. These values are then employed to implement the required corrective measures.

$$\begin{cases} x_b = x_a + \Delta x + \varepsilon_x \bullet t \\ y_b = y_a + \Delta y + \varepsilon_y \bullet t \\ z_b = z_a + \varepsilon_z \bullet t \end{cases} \tag{3}$$

The LIBS and the Gocator are both affixed to the same framework, with their relative positions meticulously pre-calibrated. This ensures that the spatial relationship between the LIBS and the Gocator remains invariant. The fixed distance between the two sensors can be used to quickly calculate and trace the correspondence between the data from each sensor. This ensures that every laser shot is accurately mapped to its corresponding surface condition data captured by the Gocator. This alignment allows for a direct and synchronized correlation between the LIBS laser shooting point and the Gocator's scanning data, which is crucial for enhancing the precision of contaminant detection in RCA streams. As illustrated in Fig. 5, a point G captured by the Gocator travels along the conveyor belt. When the LIBS is set to emit the laser after 6025 pulses, the target point G shifts to a new position, denoted as L′, due to certain deviations. At this precise moment, the actual shooting point of the LIBS laser is at L, corresponding to the point G′ previously scanned by the Gocator. The spatial correlation of points L and G′ are related as follows:

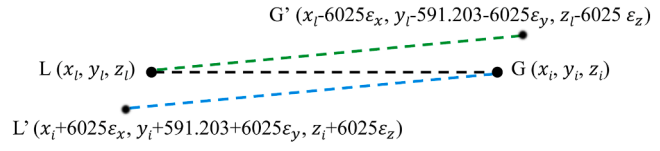

Fig. 5. Correlation between the LIBS laser shooting point and the Gocator's scanning data.

$$\begin{cases} x_l = x_i \\ y_l = y_i + 591.203 \\ z_l = z_i \end{cases} \tag{4}$$

After correction, it can be calculated that the actual corresponding point G′ for the LIBS laser shooting point L is located at the coordinates (x_i-6025ε_x, y_i-6025ε_y, z_i-6025ε_z). This representation effectively maps the corrected laser shooting point to the scanner's coordinate system, ensuring precise spatial alignment and data integration.

2.3. Analysis methods

2.3.1. Calculation of 3D point cloud normal vector

Analyzing the surface condition of objects at laser shooting points requires the determination of the object's surface normal. This step aids in calculating the laser shot's angle of incidence relative to the object's surface. In this study, a hybrid approach is used to estimate normal vectors within 3D point clouds. This method synergistically combines fixed-radius and K-Nearest neighbors (KNN) algorithms (Corral and Almendros-Jiménez, 2007) to calculate within the smallest possible range around a target point, enabling efficient and precise identification of each point's geometric characteristics in the cloud.

2.3.1.1. Neighborhood definition. The initial step involves defining each point's neighborhood using a set radius. Given a point P_u with coordinates (x_u, y_u, z_u) in the 3D point cloud, the neighborhood $N(P_u)$ of P_u within a starting radius r is defined as:

$$N(P_u) = \left\{ P_v \middle| \sqrt{(x_u - x_v)^2 + (y_u - y_v)^2 + (z_u - z_v)^2} \le r, \quad \forall u \ne v \right\} \tag{5}$$

where P_v are the points in the point clouds. Considering resolutions along the x, y, and z axes of 0.378 mm, 0.393 mm, and 0.083 mm, respectively, the starting radius r of 1 mm is set to guarantee a uniform search area, regardless of point density variations. This radius-based search encompasses all points within the specified boundary, providing a comprehensive dataset for further analysis.

2.3.1.2. Refinement to K-nearest neighbors. From the initial neighborhood $N(P_u)$, the set is refined to the k-nearest neighbors, constrained to a maximum count based on the Euclidean distance - in this case, $k = 9$. This refined neighborhood is denoted as $N_k(P_u)$.

2.3.1.3. Covariance matrix computation. Upon identifying the relevant neighborhood points, for each point P_u and its neighborhood $N_k(P_u)$, calculate the covariance matrix CM_{P_u} as:

$$CM_{P_u} = \frac{1}{k} \sum_{P_v \in N_k(P_u)} (P_v - \overline{P_u})(P_v - \overline{P_u})^T \tag{6}$$

where $\overline{P_u}$ is the centroid of the neighborhood points and is given by:

$$\overline{P_u} = \frac{1}{k} \sum_{P_v \in N_k(P_u)} P_v \tag{7}$$

This covariance matrix captures the spatial distribution of the points, forming the basis for the next steps.

2.3.1.4. Eigenvalue decomposition. The core of the normal vector estimation process involves the eigenvalue decomposition of the covariance matrix CM_{P_u}. Through this decomposition, eigenvalues φ_1, φ_2, φ_3 and their corresponding eigenvectors $\overrightarrow{\tau_1}$, $\overrightarrow{\tau_2}$, $\overrightarrow{\tau_3}$ are obtained. Eigenvectors signify the predominant axes of the point distribution. The eigenvalues are ordered as $\varphi_1 \geq \varphi_2 \geq \varphi_3$.

2.3.1.5. Normal vector estimation. The normal vector $\overrightarrow{N_u}$ at point P_u is the eigenvector $\overrightarrow{\tau_3}$ corresponding to the smallest eigenvalue φ_3, thus:

$$\overrightarrow{N_u} = \overrightarrow{\tau_3} \tag{8}$$

This choice is grounded in the principle that the smallest eigenvalue's direction exhibits the least variance, aligning with the surface normal.

2.3.1.6. Preprocessing for noise and outliers. It is imperative to recognize that irregularities in point cloud density, along with noise and outliers, can significantly affect the accuracy of normal vector estimation. When the scanning laser of the Gocator encounters gaps between particles, particularly in areas that are deeper and darker than the surrounding particle surface, the scanning laser's reflectivity may decrease. This reduction in reflectivity results in abnormal elevation data, often producing negative values. Such anomalies can introduce substantial errors in normal vector estimation, especially when calculating the boundary points of particles based on adjacent data. To enhance the reliability of the results, preprocessing steps such as noise filtering and smoothing are essential.

It is important to emphasize that these preprocessing steps are specifically designed for the normal vector estimation process. When processing LIBS spectral data later, the original Gocator scanning data, including any negative elevation values, should still be used. The presence of these negative elevation data indicates the areas where gaps between particles exist, and accurately identifying these areas is critical for subsequent corrections in LIBS spectral data analysis.

2.3.2. Surface-condition-adaptive classification algorithm

The quality of the detected spectrum is highly influenced by two factors: the distance of the focal point of the laser to the object's surface and the laser shot's angle of incidence relative to the object's surface normal during laser shooting. To ensure optimal analysis, it is essential to exclude spectral data obtained outside the focal length. Moreover, incorporating the angle values into the spectral data analysis improves accuracy. By integrating these angle values as parameters, the performance of the classification algorithm is refined and enhanced.

The surface-condition-adaptive classification algorithm for analyzing single-shot spectral data utilizes chemometric methods that integrate principal component analysis with the chi-square distribution (Chang et al., 2022). To effectively perform principal component analysis (PCA), distinct preprocessing methods are required for angle values and spectral values. This ensures comparability in magnitude and optimal representation of each data set's characteristics. For angle values, normalization is applied. Given their range of 0 to 90 degrees, they are normalized to a scale of 0 to 1. This is achieved by employing Min-Max Normalization for each angle value. This transformation maintains the proportional relationships while making the values more manageable. In contrast, spectral values are processed through standardization. The key information in spectral data, the distribution patterns of peaks and troughs, is best captured by z-score standardization. This approach maintains the data's overall distribution but adjusts the mean and standard deviation to a zero mean and unit standard deviation. By doing so, spectral values are effectively scaled, ensuring a standardized framework for further analysis.

When shooting material X, each laser shot yields an angle of incidence value d, and a corresponding spectrum $x = (x_1, x_2, \ldots, x_N)$, where x_s denotes the plasma emission intensity at wavelength $\lambda_s (s = 1, 2, \ldots, N)$, with N representing the total number of recorded spectral wavelengths. By assessing the angle of incidence and the actual focal length, spectra that do not meet the criteria are filtered out. Subsequently, by combining the normalized angle value d' with the spectrum x, a composite value $C = (d', x_1, x_2, \ldots, x_N)$ is created. Consequently, each laser shot can be considered as a point in an $N+1$ dimensional space. In this space, laser shots from the same material form a unique group of point clouds. Different materials are represented by distinct groups of point clouds. Each new laser shot creates a new point, which is either assigned to an existing point cloud group or labeled as unrecognizable if it significantly deviates from known groups.

After PCA processing, the database for material X records a selected principal component number n. This corresponds to a new, rotated orthonormal coordinate system with axes aligned along n unit vectors $(e_1, e_2, \ldots, e_n)$. The database also includes a set of vectors of principal components $(\xi_1, \xi_2, \ldots, \xi_n)$, and a center point $(\overline{\xi_1}, \overline{\xi_2}, \ldots, \overline{\xi_n})$ along with variances $\left(\overline{\Delta\xi_1{}^2}, \overline{\Delta\xi_2{}^2}, \ldots, \overline{\Delta\xi_n{}^2}\right)$ to describe the multi-dimensional normal distribution of the spectra for material X.

Following the process of z-score normalization, for each principal component value $Z_m \quad (m = 1, 2, \ldots, n)$, calculated from the obtained principal components $(\xi_1, \xi_2, \ldots, \xi_n)$, it's presumed to align with chi-square distributions for categorization purposes. Specifically, each Z_m is calculated by the equation:

$$Z_m = \frac{\xi_m - \overline{\xi_m}}{\sqrt{\overline{\Delta\xi_m{}^2}}} \tag{9}$$

showing that it conforms to a standard normal distribution, characterized by a zero mean and unit variance. Leveraging the chi-square distribution framework, the statistic:

$$\chi^2 = \sum\nolimits_1^n Z_m{}^2 = \sum\nolimits_1^n \frac{\left(\xi_m - \overline{\xi_m}\right)^2}{\overline{\Delta\xi_m{}^2}} \tag{10}$$

is scrutinized to verify its alignment with the expected $\chi_n{}^2$-distribution by checking if it is adequately small. This χ^2 metric is then converted into a probability p-value reflective of the $\chi_n{}^2$-distribution, with an inverse relationship between χ^2 and the p-value indicating an increased confidence level. A p-value below a selected significance level suggests significant statistical relevance. This significance level for material X is

set based on its associated p-value, categorizing spectra with p-values exceeding this significance level as attributable to material X.

2.3.3. Quality control method

Algorithm 1. Quality control module

Input: Laser shooting point P_u (x_u, y_u, z_u) and spectrum x
Output: Estimated content CE of each material type X_{md}

If $z_u < 0$ **then**
  Delete spectrum x
Else
  $z \leftarrow$ Calculate the corresponding z-value at the point P_u
  $d \leftarrow$ Calculate the angle of incidence at the point P_u
  If $z > focal\ length\ limit$ ***or*** $d > angle\ of\ incidence\ limit$ **then**
    Delete spectrum x
  Else
    $d' \leftarrow$ Apply Min-Max normalization to d
    $x' \leftarrow$ Apply z-score standardization to x
    $C \leftarrow$ Combine d' and x'
    For each material database X_{md} $(md = 1,2,\ldots,10)$ **do**
      $(\xi_1, \xi_2, \ldots, \xi_n) \leftarrow$ Apply PCA to C
      $Z_m = \frac{\xi_m - \overline{\xi_m}}{\sqrt{\overline{\Delta\xi_m{}^2}}} (m = 1,2,\ldots,n)$
      p -value $\leftarrow \chi^2 = \sum_1^n Z_m{}^2 = \sum_1^n \frac{\left(\xi_m - \overline{\xi_m}\right)^2}{\overline{\Delta\xi_m{}^2}}$
      If $p <$ significance level **then**
        Spectrum x is classified as the material type X_{md}
      Else
        Spectrum x is classified as not the material type X_{md}
      End If
    End For
  End If
End If
Initiate Frequency summary process
Set fixed intervals FI for summarization
For each interval $fi \in FI$ **do**
  Initialize frequency count FC_{md} for each material type X_{md}
  For each classification result within the interval fi **do**
    Increment the frequency count FC_{md} for the corresponding material type X_{md}
  End For
  Calculate the content estimate CE_{md} for each material type X_{md}
  Store the content estimate CE_{md}
End For
Aggregate all interval content estimates CE_{md} to obtain the total estimated content CE
Return Estimated content CE for each material type
End frequency summary process

Initially, the RCA is thoroughly mixed to ensure a uniform distribution. This homogeneity is achieved through the utilization of the feeder mechanism, which evenly disperses the RCA onto the conveyor belt, preparing it for further analysis. Subsequently, the Gocator continuously scans the surface of the RCA streams, calculating and detecting vital parameters such as the actual focal length (corresponding z-values z) and the angle of incidence d in real time. These measurements are crucial for the accurate classification of material types.

Parallel to the scanning process, LIBS targets fixed points on the RCA streams, shooting continuously. It integrates the obtained spectral data x with the previously calculated focal length and angle of incidence to identify the material accurately. This classification process is enhanced by periodically summarizing the frequency of occurrence FC_{md} for each material type X_{md} within fixed intervals FI, thereby estimating the content CE_{md} of various materials in the RCA streams rapidly and efficiently. The specific quality control process is outlined in Algorithm 1.

The quantified material content data is then synchronized to the cloud in real time, allowing for immediate access and analysis. This capability is instrumental in maintaining quality control, as it facilitates the quick classification of any material content that exceeds predefined limits. Once an anomaly is detected, the system enables swift marking and manual intervention, ensuring that only materials meeting the desired specifications are utilized.

3. Results and discussion

3.1. Effects of focal length

To determine the effective focal length of the LIBS system, it is essential first to calculate the diameter w_0 of the focal spot. This is achieved using Formula (11):

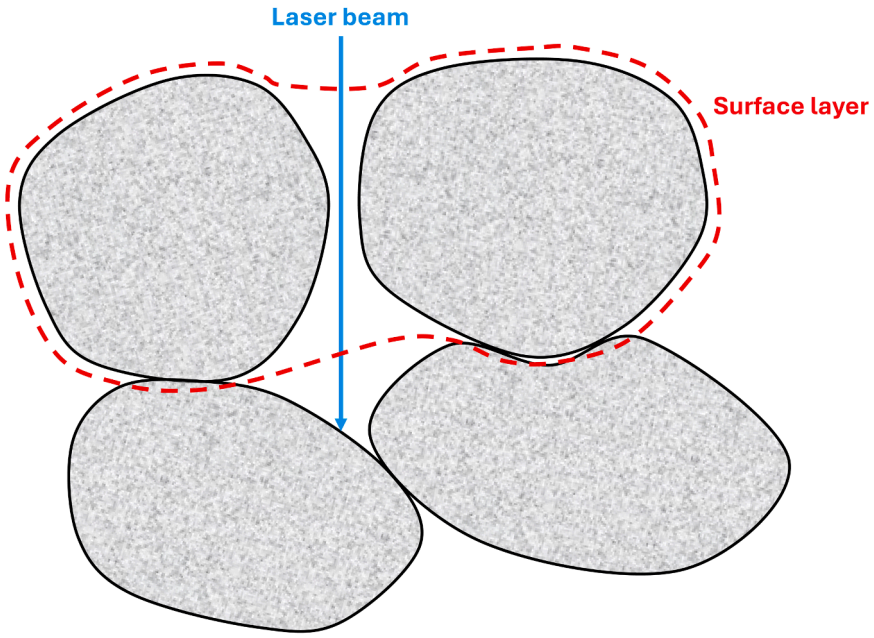

Fig. 6. Laser shoots the gap between two particles.

$$w_0 = \frac{2M^2\lambda f}{\pi D} \tag{11}$$

Formula (11) is employed to determine the $1/e^2$ spot diameter for a collimated Gaussian beam (Dickey, 2018). This beam is characterized by a wavelength λ and a diameter D at the lens when it is focused using a lens with a focal length f. If the beam deviates from an ideal Gaussian, the beam quality parameter M^2 is introduced to adjust the calculation. In this LIBS system, the parameters are $\lambda = 1064$ nm, $D = 2.5$ mm, $f = 300$ mm, and $M^2 = 1.2$. With these parameters, the calculated diameter w_0 of the focal spot is 195.1 μm.

The effective focal length range is defined by the depth of field (DOF) of the focused beam, calculated as twice the Rayleigh range Z_R:

$$\mathrm{DOF} = 2Z_R \tag{12}$$

The Rayleigh range (Herman and Wiggins, 1998), a pivotal concept in optics and laser physics, describes the characteristics of a Gaussian beam. It is the distance from the beam's narrowest point (the beam waist) to the point where the beam's diameter increases by a factor of $\sqrt{2}$. Within this distance, the beam is considered to be approximately collimated, meaning that the spread of the beam is very minimal. The mathematical expression for the Rayleigh range is typically:

$$Z_R = \frac{\pi w_0^2}{M^2\lambda} \tag{13}$$

where the parameter M^2 is included to accommodate for the increased divergence in non-ideal beams. In this study, Z_R is calculated to be 23.4 mm. It is noteworthy that within the Rayleigh range, the beam's expansion is negligible, indicating that the beam maintains almost the same intensity. Beyond this range, however, the beam starts to diverge more significantly.

Experimental results from various materials reveal that optimal spectra can be successfully obtained within a 30.0 mm distance from the focal point. Thus, a focal length range of 23.4 mm is identified as the optimal limit for effective spectral acquisition. This conclusion draws upon both empirical evidence and theoretical analysis, which shows that this specific focal distance consistently produces the most accurate and reliable spectral data across different material types, enhancing the precision of the spectroscopic analysis.

Considering the size of the measured particles, which are all smaller than 23.4 mm, it is reasonable to assume that laser shooting points are typically within the effective focal length. However, there is a possibility that the laser shoots may pass through the gap between two surface particles, penetrating below the surface layer, which is the outermost layer of the particle pile, as illustrated in Fig. 6. Laser shots in such scenarios, potentially beyond the Rayleigh range, are challenging to evaluate. This is also reflected in the Gocator scanning data, where the

Table 1
Classification report of the validation set without consideration of surface information.

	Precision	Recall	F1-score	Support
Brick	0.98	0.97	0.98	100
Cement Paste	0.98	0.94	0.96	100
Foam	1.00	0.94	0.97	100
Glass	0.98	0.98	0.98	100
Gypsum	1.00	0.97	0.99	100
Mineral Fiber	1.00	0.97	0.99	100
Plastic	0.94	0.98	0.96	100
RCA	0.91	0.93	0.92	100
RFA	0.94	0.96	0.95	100
Wood	1.00	0.96	0.98	100
Unrecognized	0.00	0.00	0.00	0
weighted avg	0.97	0.96	0.96	1000

Table 2
Classification report of the validation set with consideration of surface information.

	Precision	Recall	F1-score	Support
Brick	1.00	1.00	1.00	100
Cement Paste	0.99	0.97	0.98	98
Foam	1.00	0.98	0.99	99
Glass	0.99	0.99	0.99	99
Gypsum	1.00	0.99	1.00	99
Mineral Fiber	1.00	0.99	0.99	99
Plastic	0.97	1.00	0.99	99
RCA	0.96	0.97	0.96	97
RFA	0.96	0.98	0.97	99
Wood	1.00	0.99	1.00	98
Unrecognized	0.00	0.00	0.00	0
weighted avg	0.99	0.99	0.99	987

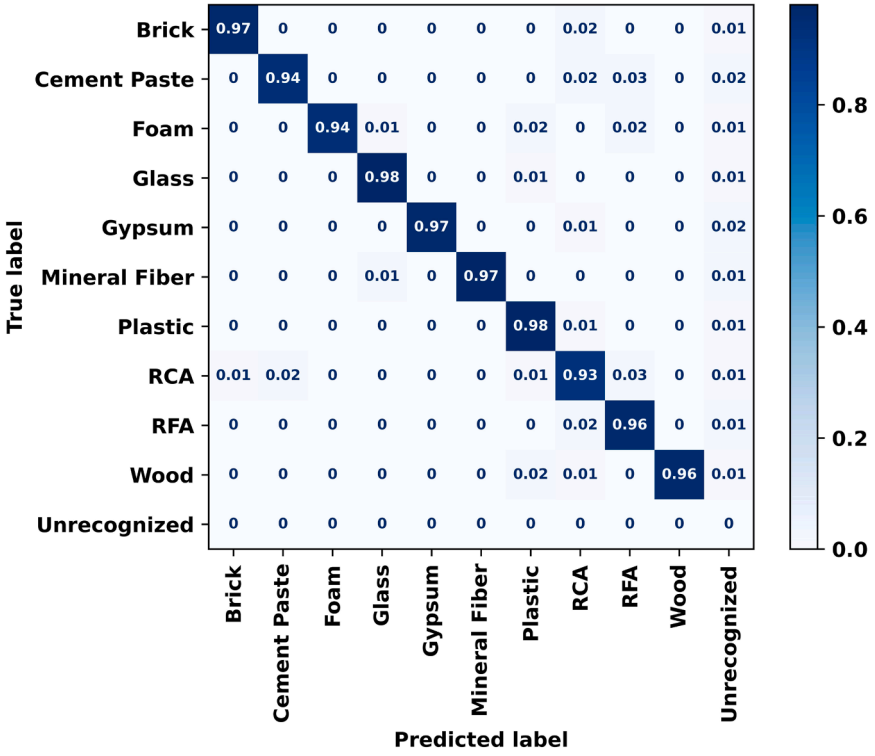

(a) Without consideration of surface information

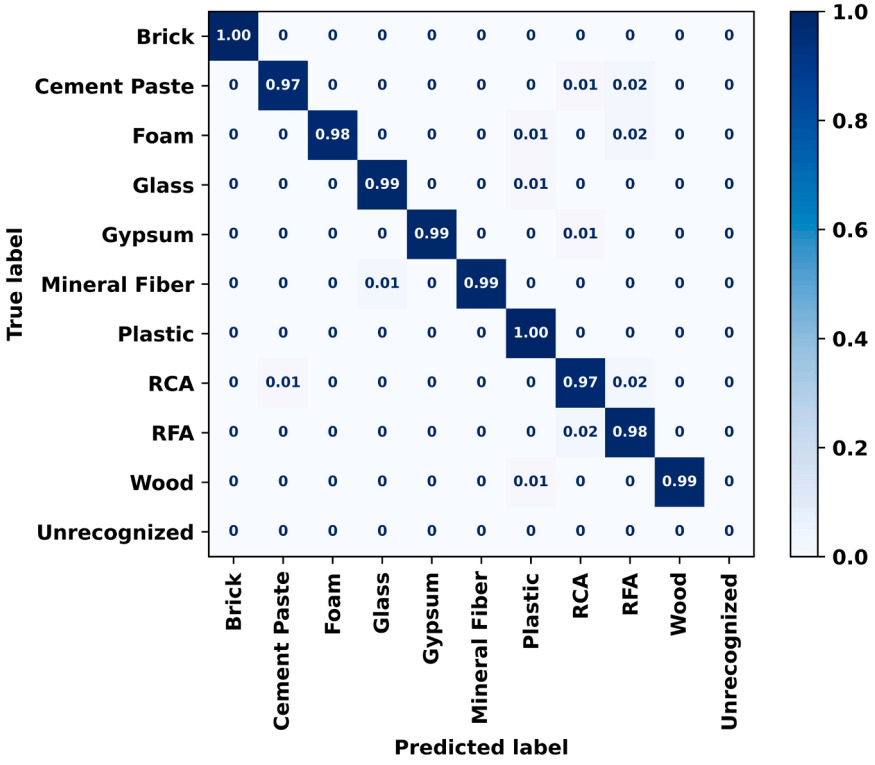

(b) With consideration of surface information

Fig. 7. Confusion matrix of the validation set.

corresponding z-values are negative. Consequently, this laser shot's incidence angle on the material's surface cannot be precisely determined. Based on this unique characteristic, these laser shot data can be excluded.

3.2. Effects of the angle of incidence

Experiments conducted on various materials revealed that optimal spectral data is obtained when the laser shot's angle of incidence is between 0 and 60 degrees relative to the object's surface normal. At angles beyond 60 degrees, spectral values tend to be significantly lower. This reduction is primarily attributed to the increased surface area impacted by the laser shots at steeper angles, leading to diminished reflected energy and consequently lower spectral values detected.

RCA tend to be more angular compared to natural aggregates. This characteristic results in highly variable surface conditions, which must be considered in their analysis. To compensate for the effect of the laser shot's incidence angle on spectral data, the angle parameter has been normalized and incorporated into the cluster-based classification algorithm. This integration allows for a more accurate analysis of the spectral data by considering the variable impact of different angles of incidence. This adjustment is crucial for improving the reliability and clarity of spectral analysis, especially in scenarios where controlling the angle of incidence is challenging.

3.3. Quality control test results

In this study, we meticulously collected data for a variety of materials, each characterized by specific angle and spectral values. To rigorously evaluate our classification methodology, we partitioned this dataset into two subsets: a training set and a validation set. The partitioning adhered to a 9:1 ratio, ensuring a balanced distribution for effective model training and validation. Specifically, for the purpose of validation, we randomly selected 100 entries for each material, resulting in a comprehensive validation set encompassing a total of 1000 entries. Conversely, the training set comprised the remaining 900 entries per material. This extensive dataset facilitated the development of a robust standard library, pivotal for the accurate classification of materials based on their spectral signatures and surface conditions.

Fig. 6 delineates the classification outcomes, offering a comparative analysis of the results obtained without considering surface conditions against those that are factored in these conditions. Further, the validation set's classification efficacy is documented in Table 1 and Table 2. These tables provide an insightful examination of the classification performance, highlighting the precision, recall, and F1 score among other metrics, thereby offering a transparent overview of our methodological accuracy and efficacy. Fig. 7

Subsequently, the constructed standard library was employed in a real-world scenario to continuously monitor the quality of RCA streams transported on the conveyor belt, following its processing through the C2CA treatment. The monitoring experiments were specifically designed to assess the content of various contaminants within the RCA streams. The experimental findings reveal that the concentration of contaminants in the RCA streams was within the permissible limits set forth by the EN 12620 standard (Standard, 2002), which delineates the requirements for aggregates to be used in concrete.

3.4. Accuracy and efficiency in quality control

Significant enhancements in the algorithm are noted when incorporating surface conditions. The algorithm with consideration of surface conditions demonstrates improvements in precision (weighted average), recall (weighted average), and F1-score (weighted average), all reaching 0.99. This is a significant advancement over the algorithm that did not account for surface conditions, which achieves a precision (weighted average) of 0.97, recall (weighted average) of 0.96, and F1-score (weighted average) of 0.96. It is important to acknowledge that the test set was approximately 40 times too small to ensure that materials, such as wood and plastics with stringent maximum concentration specifications, can be detected at the highest quality limit levels (0.1 cm^3 per kg, or about 1 in 4000 particles).

Nevertheless, the system has demonstrated high efficiency, accuracy, and significant market potential. It can monitor the quality of RCA flows at a throughput of 50 tons per hour per conveyor, analyzing approximately 4000 particles per ton of RCA. This allows the system to detect critical contaminants at concentrations below 50 parts per million. For materials with stringent content regulations, such as wood, the system can meet the required limit of 0.2 cm^3/kg, equivalent to about 0.08 g/kg or a mass concentration of 80 ppm, further demonstrating its reliability.

Notably, the most significant improvements include the complete elimination of the unrecognized category and a reduction in confusion primarily to materials with similar chemical compositions. These improvements are highlighted by the disappearance of previously unrecognized classifications and the significant reduction in misclassifications involving materials with similar chemistry, particularly where RCA was previously misclassified as other materials.

Specifically, the improvements include both the removal of previously unrecognized laser shots and a reduction in misclassifications. The elimination of these previously unrecognized laser shots arises from two factors. Firstly, it is evident that some ineffective data have been removed from various materials (except for brick). This is attributed to the probability of laser shooting the gaps between particles during consecutive laser shots. These laser shots are highly beyond the focal point, resulting in the exclusion of previously unrecognized laser shots. Secondly, the incorporation of the angle parameter aids in identifying and correcting these unrecognized laser shots. A notable instance of this improvement is observed in the case of brick. Analysis of prior literature (Chang et al., 2022) reveals that misclassified laser shots typically display smaller scales than normal and are obscured by typical values. The diminished spectral values of these laser shots, possibly caused by the angle of incidence issues, make classification challenging. By incorporating the angle of incidence of laser shots into the algorithm, these small-scale shots can be accurately identified and classified, leading to a decrease in misclassifications.

However, RCA, RFA, and cement paste remain susceptible to classification errors. Challenges arise from multiple factors. One major issue is the difficulty of ensuring the complete removal of residues during the material processing stage. In particular, the adhesion of cement paste to RCA surfaces complicates differentiation. Additionally, the size overlap between RCA and RFA, both sharing a boundary at 4.0 mm, further complicates their distinction, especially in this marginal size range where they exhibit greater similarity. The inherent heterogeneity of the materials adds another layer of complexity to the classification task. Moreover, the chemical compositional similarities among RCA, RFA, and cement paste amplify the presence of misclassifications. RCA, obtained by crushing concrete from demolished structures, generally consists of larger fragments of original aggregates, such as gravel or crushed stone, along with adhered mortar. Its chemical composition is primarily characterized by calcium oxide (CaO), silicon dioxide (SiO_2), aluminum oxide (Al_2O_3), iron oxide (Fe_2O_3), and magnesium oxide (MgO). The presence of residual mortar in RCA introduces additional variability in its chemical profile, distinguishing it from natural aggregates. In contrast, RFA, which comes from the finer fractions of the same source as RCA, consists of sand-sized material and finer residues from the original concrete. Although the chemical composition of RFA is similar to that of RCA, it contains higher proportions of calcium hydroxide [$Ca(OH)_2$] and other hydrated compounds due to its finer particle size and greater surface area. Cement paste, which acts as the binding phase in concrete, mainly consists of calcium silicate hydrate (C-S-H), calcium hydroxide, and unhydrated cement particles, with a notable presence of calcium carbonate ($CaCO_3$) due to carbonation. The similar yet heterogeneous chemical compositions of RCA and RFA lead

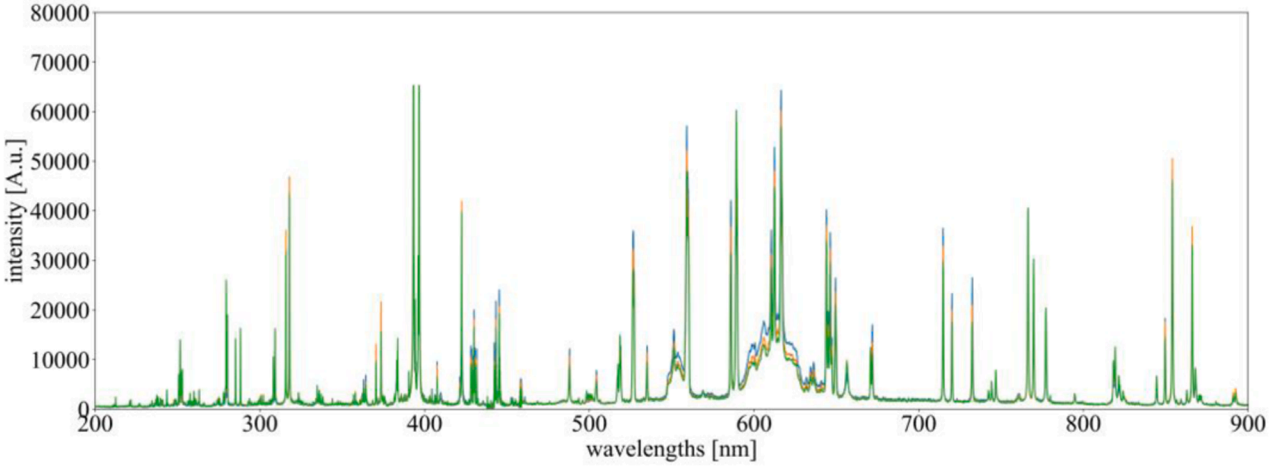

(a) RCA

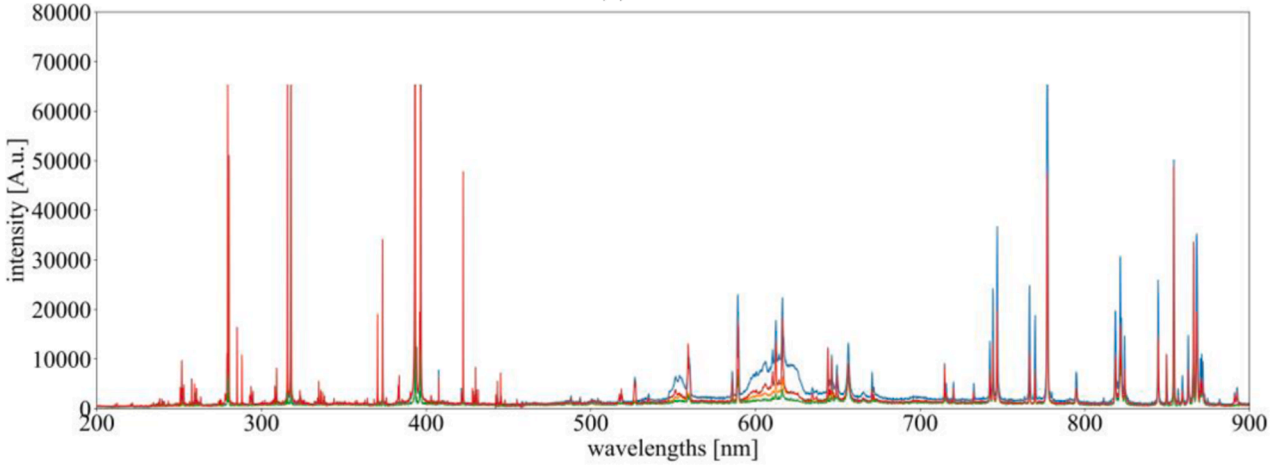

(b) RFA

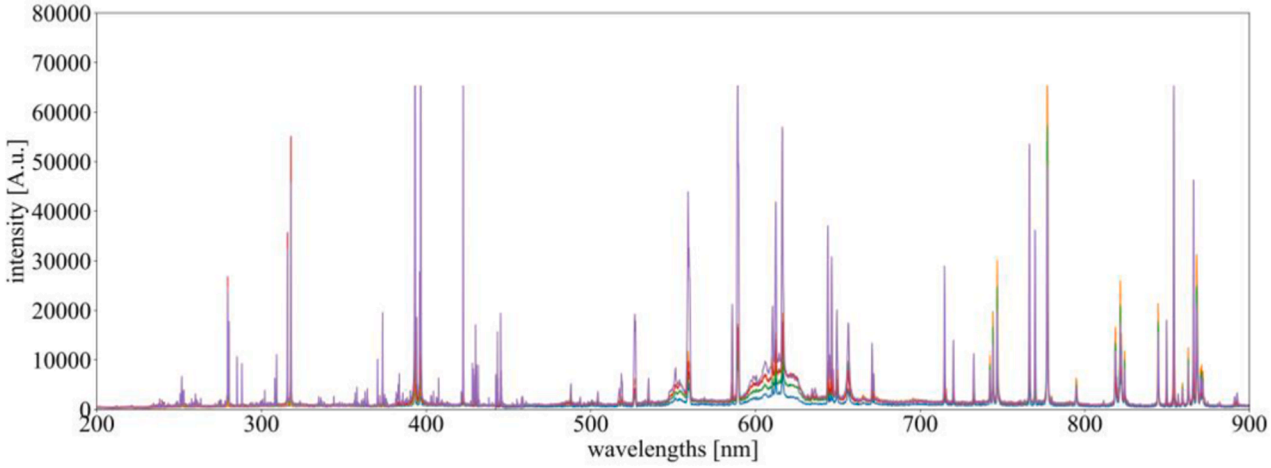

(c) Cement paste

Fig. 8. LIBS data.

to minimal differences in their spectral signatures (as shown in Fig. 8) when analyzed using LIBS. These inconsistencies in data acquisition complicate the development of a reliable database, as the collected spectra may not accurately represent the material's true characteristics. Consequently, this leads to reduced recognition accuracy when these databases are used for material classification. To overcome these challenges, more precise analysis and algorithms are necessary to improve accuracy.

Several strategies can enhance classification effectiveness. Exploring alternative methods, such as the integration of additional sensors (e.g., moisture sensors) and considering scale differences in classification, could lead to improved outcomes. The integration of machine vision (Buchner et al., 2023; Guirguis et al., 2024; Kong, 2023) could further improve the adaptability of the system by enabling real-time adjustments based on visual data, thereby enhancing the accuracy of contaminant detection in RCA streams. Alternatively, increasing the ratio of training and validation and using a greater number of spectral data for database construction can align data distribution more closely with a normal distribution. This alignment is beneficial for PCA, resulting in more accurate predictions. Therefore, extensive future experimentation is recommended to develop a robust database and improve overall accuracy.

3.5. Economic feasibility

This quality control system is designed for a plant that processes approximately 150 tons per hour of EoL concrete. Similar plants in Europe typically operate around 4000 h per year, with downtime ranging from 10 % to 20 %. To justify the investment, the system needs to process 500,000 tons annually. The facility cost is approximately €300,000, which equates to an additional 0.60 euro/ton of input material or around 1.00 euro/ton for RCA and RFA if the facility is to break even within one year. Given that typical aggregate prices in the EU range from 10.00 to 15.00 euro/ton, investing in a quality control system that not only ensures product quality but also supports a digital concrete recycling process and reduces labor costs is economically feasible.

3.6. Control model

To effectively manage the sensor-based quality control system integrating the 3D scanner Gocator and LIBS, a comprehensive control model is essential, especially in future real-world production scenarios. This model will facilitate real-time monitoring, support decision-making, and allow for process adjustments, ensuring consistent product quality. Below is a brief overview of the relevant aspects of the control model.

3.6.1. Control objectives

The primary objectives of the control model are:

Real-time monitoring: Continuously monitor the quality parameters as measured by the Gocator and LIBS.

Process adjustment: Automatically adjust production parameters based on the quality data to maintain product specifications.

Feedback loop: Implement a feedback mechanism to refine the control model based on performance data and operational changes.

3.6.2. Control model components

3.6.2.1. Data acquisition and integration. Sensors: The Gocator and LIBS are used to acquire dimensional and compositional data, respectively. The data is collected in real time and integrated into the control system.

Data fusion: Combine data from both sensors to provide a comprehensive view of product quality. This involves aligning and synchronizing data streams from the Gocator and LIBS.

3.6.2.2. Control algorithms. Algorithm selection: Employ control algorithms such as Proportional-Integral-Derivative (PID) control and Model Predictive Control (MPC) based on the complexity and requirements of the control system.

PID control: Adjusts production parameters based on the difference between the measured values and target values. It is suitable for systems with stable and predictable dynamics.

MPC: Uses a model of the system to predict future behavior and optimize control actions. It is useful for handling constraints and managing more complex systems.

3.6.2.3. Feedback mechanism. Real-time feedback: Implement a feedback loop that uses data from the Gocator and LIBS to adjust process parameters. For example, if the Gocator detects dimensional deviations, the system can adjust machine settings to correct these deviations.

Error correction: Apply corrective actions when deviations from quality standards are detected. This involves updating control parameters and re-calibrating processes as needed.

3.6.2.4. Control Model Implementation. Software integration: Develop or integrate control software that processes sensor data and executes control algorithms. The software should interface with both the Gocator and LIBS systems.

User interface: Provide an intuitive user interface for operators to monitor system performance, review data, and manually adjust parameters if necessary.

3.6.3. Model validation and testing

3.6.3.1. Simulation. Simulation setup: Before implementing the control model in a live environment, simulate the model using historical data to validate its performance and accuracy.

Scenario testing: Test the control model under various scenarios, including different levels of input quality and varying production conditions, to ensure robustness.

3.6.3.2. Experimental validation. Pilot testing: Implement the control model in a pilot production run to observe its performance in a real-world setting.

Performance metrics: Evaluate the control model based on key performance indicators (KPIs) such as response time, accuracy of adjustments, and overall impact on product quality.

3.6.3.3. Continuous improvement. Performance monitoring: Continuously monitor the performance of the control model during production. Collect feedback on its effectiveness and identify areas for improvement.

Model refinement: Use performance data to refine and enhance the control model. This may involve adjusting control algorithms, recalibrating sensors, or improving data integration methods.

4. Conclusion

This study introduces a novel rapid quality control system for contaminant detection in RCA streams via surface-condition-adaptive LIBS. A key advancement is the integration of a synchronized system that merges spatial data from a 3D scanner with the spectral data from LIBS. This novel approach effectively tackles the issue of variable surface conditions on objects, which affect the laser shot's focal length and angle of incidence. These factors have previously impeded the precision of traditional LIBS applications. By adapting the spectra based on the surface position and orientation, as determined by 3D scanning, this method significantly reduces unrecognizable classifications and misclassification rates, enhancing the reliability of material classification. The surface-condition-adaptive LIBS method demonstrates improvements in precision (weighted average), recall (weighted average),

and F1-score (weighted average), all reaching 0.99. This level of accuracy is pivotal for the rapid quality control of RCA streams on the conveyor belt, underpinning its utility in ensuring the quality of RCA utilized in construction projects.

The advancements of this study enhance the reliability of single-shot analyses of LIBS, thereby reducing the occurrence of false positives during the material classification process. In situations where the concentration of contaminants is extremely low, false positives can significantly influence the results of theoretical simulations. For example, with a 1 % wood content that is uniformly distributed, the likelihood of detecting wood is only once in every 100 samples. However, false positives in other materials could falsely inflate the estimated wood content, greatly impacting the quality assessment of RCA. By precisely adjusting the angle of incidence and eliminating spectra outside the focal range, the quality of the spectra has been improved, and the incidence of false positives has been substantially lowered. This enhancement is essential for preserving the integrity and reliability of recycling processes.

This study highlights the potential of surface characterizing in the recognition of different materials. The diversity in surface properties of different materials presents a unique opportunity for precision in material classification. Detailed analysis of these surface characteristics, combined with existing technologies, enables more accurate recognition of various materials. The integration of 3D scanning with LIBS allows for a detailed understanding of surface conditions, which plays a pivotal role in enhancing the accuracy of material classification. This research underscores the significance of surface properties in the classification process and paves the way for further advancements in material recognition technology. Moreover, future research should investigate automated analysis techniques for discerning particle size distributions in different materials. The use of advanced sensors allows for the swift collection of particle size data of a specific material in mixed material streams, augmenting the efficiency and precision of recycling processes.

Beyond waste management and recycling, this research has broader implications across various industries where material classification and detection of particle flows are pivotal. However, the study also acknowledges the complexities in distinguishing materials with similar spectral signatures. The challenge remains in fine-tuning the LIBS methodology to distinguish between such materials with greater specificity. Future research could focus on enhancing the algorithmic aspect of LIBS data interpretation, potentially incorporating machine learning techniques to refine the classification process. Moreover, exploring the synergy of LIBS with other analytical techniques, such as Micro-electromechanical Systems (MEMS)-based sensors (Grosse et al., 2006; He, 2024; He et al., 2024), could offer a more comprehensive understanding of material classification and detection.

While our research provides a comprehensive solution for quality control, we acknowledge that there are additional areas that warrant further investigation. One such area is the optimization of scheduling for RCA streams. Developing an optimal scheduling model for RCA involves complex considerations including inventory management, production requirements, and material quality control. Given the importance of efficient resource utilization and the potential benefits of improved scheduling, this is a promising area for future research. An optimal scheduling approach could leverage advanced algorithms and optimization techniques to balance RCA usage with production needs effectively. Such a model could enhance overall efficiency and reduce waste, addressing a critical aspect of resource management in civil engineering materials.

Importantly, this study has broader implications for environmental sustainability. It exemplifies the potential of combining advanced scanning and spectroscopy technologies with real-time data analysis and cloud synchronization to enhance construction material recycling processes. Through the rapid quality control of RCA streams, it promotes more efficient recycling of construction waste, thereby reducing the environmental impact of building materials and prompting their use in the building sector. This approach aligns with global efforts towards circular economies, where maximizing the reuse and recycling of materials is paramount.

CRediT authorship contribution statement

Cheng Chang: Writing – original draft, Visualization, Validation, Software, Methodology, Investigation, Formal analysis, Data curation, Conceptualization. **Francesco Di Maio:** Writing – review & editing, Supervision, Project administration, Methodology, Funding acquisition, Conceptualization. **Rajeev Bheemireddy:** Software, Data curation. **Perry Posthoorn:** Software, Data curation. **Abraham T. Gebremariam:** Writing – review & editing, Resources. **Peter Rem:** Writing – review & editing, Supervision, Project administration, Methodology, Funding acquisition, Conceptualization.

Declaration of Competing Interest

The authors declare that they have no known competing financial interests or personal relationships that could have appeared to influence the work reported in this paper.

Data Availability

Data will be made available on request.

Acknowledgements

Fundings: This work was supported by the European Union's Horizon 2020 funded Project " Innovative Circular Economy Based solutions demonstrating the Efficient Recovery of valuable material resources from the Generation of representative end-of-life building materials" (ICEBERG, grant agreement No. 869336).

References

Abid, S.R., Nahhab, A.H., Al-aayedi, H.K.H., Nuhair, A.M., 2018. Expansion and strength properties of concrete containing contaminated recycled concrete aggregate. Case Stud. Constr. Mater. 9, e00201. https://doi.org/10.1016/J.CSCM.2018.E00201.

Ahmad, S., Upadhyay, S., Umar, A., Al-Osta, M.A., 2023. Effect of recycled crushed glass and recycled coarse aggregate on the properties of self-compacting concrete. Case Stud. Constr. Mater. 19, e02532. https://doi.org/10.1016/J.CSCM.2023.E02532.

Bai, G., Zhu, C., Liu, C., Liu, B., 2020. An evaluation of the recycled aggregate characteristics and the recycled aggregate concrete mechanical properties. Constr. Build Mater. 240, 117978. https://doi.org/10.1016/J.CONBUILDMAT.2019.117978.

Bonifazi, G., Palmieri, R., Serranti, S., 2018. Evaluation of attached mortar on recycled concrete aggregates by hyperspectral imaging. Constr. Build Mater. 169, 835–842. https://doi.org/10.1016/J.CONBUILDMAT.2018.03.048.

Buchner, T.J.K., Rogler, S., Weirich, S., Armati, Y., Cangan, B.G., Ramos, J., Twiddy, S.T., Marini, D.M., Weber, A., Chen, D., Ellson, G., Jacob, J., Zengerle, W., Katalichenko, D., Keny, C., Matusik, W., Katzschmann, R.K., 2023. Vision-controlled jetting for composite systems and robots. Nature 623, 522–530. https://doi.org/10.1038/s41586-023-06684-3.

Cabral, J.S., Menegatti, C.R., Nicolodelli, G., 2023. Laser-induced breakdown spectroscopy in cementitious materials: a chronological review of cement and concrete from the last 20 years. TrAC Trends Anal.. Chem. 160, 116948. https://doi.org/10.1016/J.TRAC.2023.116948.

Caiazzo, B., Di Nardo, M., Murino, T., Petrillo, A., Piccirillo, G., Santini, S., 2022. Towards Zero Defect Manufacturing paradigm: a review of the state-of-the-art methods and open challenges. Comput. Ind. 134, 103548. https://doi.org/10.1016/J.COMPIND.2021.103548.

Chang, C., Maio, F.Di, Rem, P., Gebremariam, A.T., Mehari, F., Xia, H., 2022. Cluster-based identification algorithm for in-line recycled concrete aggregates characterization using Laser-Induced Breakdown Spectroscopy (LIBS). Resour. Conserv. Recycl. 185, 106507. https://doi.org/10.1016/J.RESCONREC.2022.106507.

Corral, A., Almendros-Jiménez, J.M., 2007. A performance comparison of distance-based query algorithms using R-trees in spatial databases. Inf Sci (N Y) 177, 2207–2237. https://doi.org/10.1016/J.INS.2006.12.012.

de Andrade Salgado, F., de Andrade Silva, F., 2022. Recycled aggregates from construction and demolition waste towards an application on structural concrete: a review. J. Build. Eng. 52, 104452. https://doi.org/10.1016/J.JOBE.2022.104452.

Dickey, F.M., 2018. Laser Beam Shaping: Theory and Techniques. CRC press.

Dietz, T., Gottlieb, C., Kohns, P., Ankerhold, G., 2019. Comparison of atomic and molecular emission in laser-induced breakdown spectroscopy for the quantification

of harmful species in cement-based materials. Spectrochim Acta Part B At Spectrosc 161, 105707. https://doi.org/10.1016/J.SAB.2019.105707.
Elfaham, M.M., Eldemerdash, U., 2019. Advanced analyses of solid waste raw materials from cement plant using dual spectroscopy techniques towards co-processing. Opt. Laser Technol. 111, 338–346. https://doi.org/10.1016/J.OPTLASTEC.2018.10.009.
Gebremariam, A.T., Di Maio, F., Vahidi, A., Rem, P., 2020. Innovative technologies for recycling End-of-Life concrete waste in the built environment. Resour. Conserv. Recycl. 163. https://doi.org/10.1016/j.resconrec.2020.104911.
Gottlieb, C., Millar, S., Grothe, S., Wilsch, G., 2017. 2D evaluation of spectral LIBS data derived from heterogeneous materials using cluster algorithm. Spectrochim Acta Part B At Spectrosc. 134, 58–68. https://doi.org/10.1016/J.SAB.2017.06.005.
Grosse, C.U., Glaser, S.D., Krüger, M., 2006. Condition monitoring of concrete structures using wireless sensor networks and MEMS. Smart Structures and Materials 2006: Sensors and Smart Structures Technologies for Civil, Mechanical, and Aerospace Systems. SPIE, pp. 407–418.
Guirguis, D., Tucker, C., Beuth, J., 2024. Accelerating process development for 3D printing of new metal alloys. Nat Commun. 15, 582. https://doi.org/10.1038/s41467-024-44783-5.
Güvenç, M.A., Bilgiç, H.H., Mıstıkoğlu, S., 2023. Identification of chatter vibrations and active vibration control by using the sliding mode controller on dry turning of titanium alloy (Ti6Al4V).
He, C.-H., Liu, H.-W., Liu, C., 2024. A fractal-based approach to the mechanical properties of recycled aggregate concretes. Facta Universitatis, Series: Mechanical Engineering.
He, J.-H., 2024. Periodic solution of a micro-electromechanical system. Facta Universitatis, Series: Mechanical Engineering.
He, J.-H., He, C.-H., Qian, M.-Y., Alsolami, A.A., 2024. Piezoelectric Biosensor based on ultrasensitive MEMS system. Sens Actuators A Phys 376, 115664.
Herman, R.M., Wiggins, T.A., 1998. Rayleigh range and the M2 factor for Bessel–Gauss beams. Appl. Opt. 37, 3398–3400. https://doi.org/10.1364/AO.37.003398.
Jia, J., Fu, H., Hou, Z., Wang, H., Ni, Z., Dong, F., 2019. Calibration curve and support vector regression methods applied for quantification of cement raw meal using laser-induced breakdown spectroscopy. Plasma Sci. Technol. 21, 034003. https://doi.org/10.1088/2058-6272/aae3e1.
Kim, C.K., In, J.H., Lee, S.H., Jeong, S., 2013. Influence of laser wavelength on the laser induced breakdown spectroscopy measurement of thin CuIn1- xGaxSe2 solar cell films. Spectrochim Acta Part B At Spectrosc. 88, 20–25. https://doi.org/10.1016/j.sab.2013.07.012.
Kong, Y.L., 2023. Multi-material 3D printing guided by machine vision.
Lux, J., Lau Hiu Hoong, J.D., Mahieux, P.Y., Turcry, P., 2023. Classification and estimation of the mass composition of recycled aggregates by deep neural networks. Comput. Ind. 148, 103889. https://doi.org/10.1016/J.COMPIND.2023.103889.
Mansoori, A., Roshanzadeh, B., Khalaji, M., Tavassoli, S.H., 2011. Quantitative analysis of cement powder by laser induced breakdown spectroscopy. Opt. Lasers Eng. 49, 318–323. https://doi.org/10.1016/J.OPTLASENG.2010.10.005.
Martín-Morales, M., Zamorano, M., Ruiz-Moyano, A., Valverde-Espinosa, I., 2011. Characterization of recycled aggregates construction and demolition waste for concrete production following the Spanish Structural Concrete Code EHE-08. Constr. Build Mater. 25, 742–748. https://doi.org/10.1016/J.CONBUILDMAT.2010.07.012.
Palanco, S., M. Cabalín, L., Romero, D., J. Laserna, J., 1999. Infrared laser ablation and atomic emission spectrometry of stainless steel at high temperatures. J. Anal. At. Spectrom. 14, 1883–1887. https://doi.org/10.1039/A905472C.
Serranti, S., Bonifazi, G., 2020. Detection and classification of asbestos and other contaminants in C&DW by advanced technologies. Advances in Construction and Demolition Waste Recycling: Management, Processing and Environmental Assessment 407–437. https://doi.org/10.1016/B978-0-12-819055-5.00020-6.
Serranti, S., Palmieri, R., Bonifazi, G., Gasbarrone, R., Hermant, G., Bréquel, H., 2023. An automated classification of recycled aggregates for the evaluation of product standard compliance. Sustainability 15, 15009. https://doi.org/10.3390/su152015009.
Silva, R.V., de Brito, J., Dhir, R.K., 2017. Availability and processing of recycled aggregates within the construction and demolition supply chain: a review. J. Clean Prod. 143, 598–614. https://doi.org/10.1016/J.JCLEPRO.2016.12.070.
Standard, B., 2002. Aggregates for concrete. BS EN 12620.
Suthar, J., Persis, J., Gupta, R., 2023. Predictive modeling of quality characteristics – a case study with the casting industry. Comput. Ind. 146, 103855. https://doi.org/10.1016/J.COMPIND.2023.103855.
Vegas, I., Broos, K., Nielsen, P., Lambertz, O., Lisbona, A., 2015. Upgrading the quality of mixed recycled aggregates from construction and demolition waste by using near-infrared sorting technology. Constr Build Mater 75, 121–128. https://doi.org/10.1016/J.CONBUILDMAT.2014.09.109.
Völker, T., Millar, S., Strangfeld, C., Wilsch, G., 2020. Identification of type of cement through laser-induced breakdown spectroscopy. Constr Build Mater 258, 120345. https://doi.org/10.1016/J.CONBUILDMAT.2020.120345.
Wang, J., Li, Xiaolong, Li, H., Li, Xinzhong, Li, Z., 2020. Lens-to-sample distance effect on the quantitative analysis of steel by laser-induced breakdown spectroscopy. J. Phys. D Appl. Phys. 53. https://doi.org/10.1088/1361-6463/ab7f74.
Wang, Z., Afgan, M.S., Gu, W., Song, Y., Wang, Y., Hou, Z., Song, W., Li, Z., 2021. Recent advances in laser-induced breakdown spectroscopy quantification: from fundamental understanding to data processing. TrAC Trends Anal. Chem. 143, 116385. https://doi.org/10.1016/J.TRAC.2021.116385.
Xia, H., Bakker, M.C.M., 2014. Reliable classification of moving waste materials with LIBS in concrete recycling. Talanta 120, 239–247. https://doi.org/10.1016/j.talanta.2013.11.082.
Yin, H., Hou, Z., Zhang, L., Zhang, X., Wang, Z., Li, Z., 2016. Cement raw material quality analysis using laser-induced breakdown spectroscopy. J. Anal. At Spectrom. 31, 2384–2390. https://doi.org/10.1039/c6ja00323k.
Yu, J., Hou, Z., Ma, Y., Li, T., Fu, Y., Wang, Y., Li, Z., Wang, Z., 2020. Improvement of laser induced breakdown spectroscopy signal using gas mixture. Spectrochim Acta Part B At Spectrosc. 174, 105992. https://doi.org/10.1016/J.SAB.2020.105992.
Zhang, Y., Jia, Y.-H., Chen, J.-W., Shen, X.-J., Zhao, L., Yang, C., Chen, Y.-Y., Zhang, Y.-H., Han, P.-C., 2012. Study on parameters influencing analytical performance of laser-induced breakdown spectroscopy. Front. Phys. (Beijing) 7, 714–720. https://doi.org/10.1007/s11467-012-0267-7.
Živković, S., Botto, A., Campanella, B., Lezzerini, M., Momčilović, M., Pagnotta, S., Palleschi, V., Poggialini, F., Legnaioli, S., 2021. Laser-Induced Breakdown Spectroscopy elemental mapping of the construction material from the Smederevo Fortress (Republic of Serbia). Spectrochim Acta Part B At Spectrosc. 181, 106219. https://doi.org/10.1016/J.SAB.2021.106219.